Nanostructured chitosan-palygorskite hybrid microspheres for controlled delivery of thymol

Materials Research Express

PAPER

Nanostructured chitosan-palygorskite hybrid microspheres for controlled delivery of thymol

W Ramos-Torres, Rocío Borges-Argáez and P I Gonzalez-Chi*

Centro de Investigación Científica de Yucatán A.C., Unidad de Materiales, Calle 43, No. 130, Col. Chuburná de Hidalgo, Mérida, Yucatán. C.P. 97200, Mexico

* Author to whom any correspondence should be addressed.

E-mail: ivan@cicy.mx

Keywords: hybrid microspheres, chitosan, palygorskite, thymol, controlled release

OPEN ACCESS

RECEIVED
20 July 2021

REVISED
16 September 2021

ACCEPTED FOR PUBLICATION
24 September 2021

PUBLISHED
26 October 2021

Abstract

Hybrid microspheres from palygorskite (PAL) nanoclay and crosslinked chitosan (QS) were prepared with the emulsion method to trap and control the release of thymol (TIM). The morphology of the microspheres was characterized by scanning electron microscopy and x-ray diffraction. The size of the microspheres, the swelling rate, the encapsulation efficiency and thymol release rate were characterized. Compared to pristine chitosan microspheres, hybrid microspheres showed the highest encapsulation efficiency. The average particle sizes of the QS and QS-PAL microspheres are in a range of 20 to 50 μm, with a size distribution of the hybrid microspheres showing less size polydispersity. The QS-PAL microspheres have a higher swelling rate than the QS microspheres. The lowest swelling degree, 88%, was from the microspheres without PAL cross-linked with 950 μl of glutaraldehyde (GL), and the highest swelling degree, 146%, was from the microspheres with 10% PAL crosslinked with 630 μl of GL. The thymol release kinetics was modified by the palygorskite content of the chitosan hybrid microspheres.

1. Introduction

The control of agricultural pests has generated regulatory measures aimed to protect the environment. Normally, herbicides, fungicides, insecticides and other synthetic biocides which alter and pollute the natural ecosystems are used to control these pests [1, 2]. Due to this problem, in the last decade, the use of products friendly to the environment has been promoted. However, pesticides do not only affect a specific pest, but also other beneficial insects such as bees. In this sense, bad pest control practices and the attack by the mite *Varroa destructor* have caused the so-called collapse of the populations of *Apis mellifera* bees [3–5].

Several synthetic acaricides based on petrochemical products have been evaluated, such as amitraz, cymiazol, fluvalinate, flumethrin, clofentezine, chlorobenzilate and coumaphos, but only some of them have been effective in controlling bee mite species [6]. In addition, synthetic acaricides can pollute honey, wax products, and Varroa mites can develop resistance to these chemicals [7]. The use of natural products for the mite control is a potential solution to this apiary problem. However, natural products are susceptible to exacerbated evaporation and present premature environmental degradation due to climatic conditions such as high temperature and relative humidity [8]. Therefore, the controlled release of acaricidal active agents from plant extracts is a possible solution since the nanostructured materials are able to protect them from the environmental factors.

Some plant extracts have essential oils that show a broad spectrum of activity against pathogenic insects, pests and fungi and can be used as insecticides, repellents, oviposition deterrents, even pest growth regulators. Recent research indicates that some chemical components of these oils interfere with the nervous system of insects; toxicological tests show that most chemical compounds from essential oils are relatively non-toxic to mammals and fish and meet the criteria to be considered low-risk pesticides. Thymol is extracted from the

essential oil of oregano (*Origanum vulgare*) and has been used to preserve food because of its antimicrobial and fungicidal activity. It has also been used to control the *Varroa Destructor* mite and as insect repellent [8–10].

The success of natural pest control products so far has been limited by several factors, for example, evaporation and degradation (photolytic, hydrolytic and microbial). These processes may eliminate the active substances before they can perform their function. In addition, there is easy availability to competitive new synthetic products, which are cost-effective and relatively safe [8, 11]. Nevertheless, the use of nanotechnology could counteract these drawbacks and increase the efficiency of these natural pesticides through modern formulation techniques. Advances in the past decade have demonstrated the controlled release of essential oils from garlic, neem seed, and *Lippia sidoides* using polyethylene glycol, chitosan, and alginate glutaraldehyde as delivery vehicles [12–14].

Chitosan, on the other hand, has multiple applications in the pharmaceutical area as a vehicle to deliver active agents. In recent years, there has been an increased development in the agricultural use of chitosan for various purposes: as a coating for seeds and their conservation and storage, as a fungicide, as a delivery vehicle to release pesticides, herbicides and fertilizers, and as an animal food additive [15]. Materials such as nanoclays have been used for nanostructured polymer composites; the main nanoclays studied have been montmorillonite (MMT) and nanosilica, although in recent years there has also been a growing interest in other clays such as palygorskite [16–18]. These nanoparticles can accommodate organic substances within their structure and function as carriers for the controlled delivery of active agents [19]. The environmental pH, the cationic groups in the chemical structure of the active agent, the cation exchange capacity, the large surface area and porosity of the nanoclays, and their dispersion control the release kinetics of the active agent [20, 21].

Chitosan-palygorskite nanostructured composites can be obtained directly by incorporating the clay into the polymer using polar solvents such as water, alcohols or nitriles, due to the interactions between the polymer functional groups (–OH, NH_2, oxyethylenes) and the clay surface [22–24]. The mechanisms of interaction between chitosan and palygorskite can be attributed to the formation of hydrogen bonds between silanol groups and water molecules on the clay surface with the hydroxyl and amino polar groups of chitosan [22, 23]. Also, they can interact through electrostatic bonds of the protonated amino group of chitosan with the clay surface. The incorporation of the clay into the chitosan modifies the release profiles of the active agent due to their interactions with the components of the composite; for example, thymol has –OH groups in its structure which can interact with clay or chitosan, improving the active agent retention in the microspheres [22, 25].

The present project proposes the study of hybrid systems of controlled release of the acaricidal agent thymol for its potential application in the field through the use of biodegradable polymers and nanoparticles of paligorskite (nanoclay-polymer-acaricidal active agent).

2. Experimental

2.1. Materials

Industrial chitosan with a deacetylation degree greater than 80% was supplied by Vepinsa. The Palygorskite clay was extracted from regional quarries located in the southwestern zone of the state of Yucatan in Mexico. The following companies supplied the materials listed: commercial thymol was purchased from Mieles Tecnología, Span-80 surfactant from Sigma Aldrich, glutaraldehyde reagent grade and acetic acid from JT Baker, and commercial liquid paraffin 55 USP (mineral oil) was obtained from Combustibles Americanos.

2.2. Emulsion method to prepare chitosan (QS) and chitosan-palygorskite (QS-PAL) microspheres

QS microspheres were prepared by dissolving 0.48 g of chitosan powder in 10 ml of a 2% (V/V) acetic acid solution, stirring at 1500 rpm and a temperature of 30 °C. The mixture was emulsified at room temperature with 15 ml of liquid paraffin and 28.2 mg of Span-80 surfactant (% w/v = 0.188). After 30 min of stirring, the microspheres obtained were cross-linked by adding glutaraldehyde (GL, 630 and 950 μl) to the emulsion at 60 °C for 3 h. Finally, the microspheres were recovered by filtration and washed with *n*-hexane for subsequent drying at 60 °C.

The QS-PAL microspheres were prepared with the method described in the previous paragraph with a palygorskite content of 2.5, 5 and 10% by weight with respect to the weight of the chitosan. The nanoclay was first mixed with the chitosan powder in a mortar and both were added to the aqueous acetic acid solution.

The conditions for the hybrid microspheres preparation were established with a complete factorial experimental design (CFD). The effect of two independent variables (factors) was studied: the palygorskite content and the relationship between the amount of glutaraldehyde and chitosan. The response variables were the size of the microspheres, the degree of swelling and the encapsulation efficiency.

2.3. Infrared spectroscopy with Fourier transform of QS, PAL and microspheres of QS and QS-PAL

The chitosan, palygorskite and the microspheres were characterized by infrared spectroscopy using KBr tablets. The analysis was carried out in a ThermoScientific™ Nicolet™ 8700 Fourier transform infrared spectrophotometer. Spectra were obtained in the range of 4000 to 400 cm^{-1} with a resolution of 4 cm^{-1}, averaging at least 100 scans.

2.4. Scanning electron microscopy (MEB) of the QS and QS-PAL microspheres

SEM images were obtained from a scanning electron microscope manufactured by JEOL, model JSM-6360 LV. Each sample was placed on a carbon tape attached to a sample holder and was subsequently introduced into a sputtering chamber for 45 s to deposit a thin layer of gold. The sample was then introduced into the vacuum chamber of the microscope. The voltage used was 20,000 V and a focal length of 3 mm.

2.5. Particle size of the QS and QS-PAL microspheres

The particle size and distribution were measured using a Coulter® LS100Q brand particle analyzer. The QS and QS-PAL microspheres were placed in a cell with ethanol and dispersed by magnetic stirring in the equipment.

2.6. Swelling degree of the QS and QS-PAL microspheres

The swelling rate of the microspheres was determined by an immersion in ethanol. 100 mg of the microspheres was placed in vials with 10 ml of ethanol at 35 °C and after 24 h of swelling, the excess of ethanol that had adhered to the surface of the microspheres was removed with absorbent paper and the microspheres were immediately weighed (W_S). Subsequently, the microspheres were dried (W_D) at 60 °C for 24 h in a convection oven. The swelling ratio was determined using the following equation:

$$S_w(\%) = ((W_S - W_d)/W_d) * 100$$

where W_S and W_d are the weights of the dry and swollen microspheres, respectively.

2.7. X-ray diffraction (XRD) of QS, PAL and QS and QS-PAL microspheres

The purified paligorskite, as well as the microspheres, were analyzed with a Siemens model D5000 x-ray diffractometer, with a CuKα anode at a wavelength of 1.54 Å, using a voltage of 34 kV and a current of 25 mA. 3 mg of each type of microsphere was deposited and compacted in a sample holder; X-ray diffraction patterns were taken at a scanning speed of 0.4° min^{-1}.

2.8. Thymol encapsulation efficiency of QS, QS-PAL microspheres

The QS and QS-PAL microspheres (table 2) were loaded with thymol (TIM) by passive absorption. Initially, a 1% thymol-ethanol solution was prepared, and the microspheres were immersed in 10 ml of this solution with a 2:1 weight ratio (microspheres:thymol), and were magnetically stirred for 24 h. The microspheres were recovered by centrifugation and washed with water. The amount of TIM absorbed by the microspheres was determined by UV-visible spectroscopy using a Thermo Scientific™ model Genesys™ 10 S spectrophotometer. 3 mg of the microspheres and 2 ml of ethanol were mixed in Eppendorf tubes and sonicated for 30 min to break the microspheres and solubilize the TIM. Subsequently, the tubes were centrifuged at 16,000 gravities for 30 min, and 700 μl of the supernatant was taken, placed in a quartz cell and absorbance at the maximum wavelength of TIM in ethanol (275 nm) was measured. Encapsulation efficiency was calculated using the following equation:

$$\%E = M_O/M_T * 100$$

where:

%E = encapsulation efficiency
M_O = encapsulated active substance weight
M_T = weight of the theoretically encapsulated active substance

2.9. Release isotherms to the environment of absorbed TIM in QS and QS-PAL microspheres

A chamber at a controlled temperature of 35 °C, equipped with an Inkbird model ITC-308 digital thermostat was used to study the controlled release of the absorbed TIM to the atmosphere. 200 mg of the microspheres was placed in the chamber and 5 mg was extracted from the chamber at certain time intervals. The quantification of TIM in the extracted microspheres was carried out with the methodology presented in section 2.9; the amount of released TIM was obtained by the difference between the initially encapsulated TIM content and the TIM remaining in the microspheres.

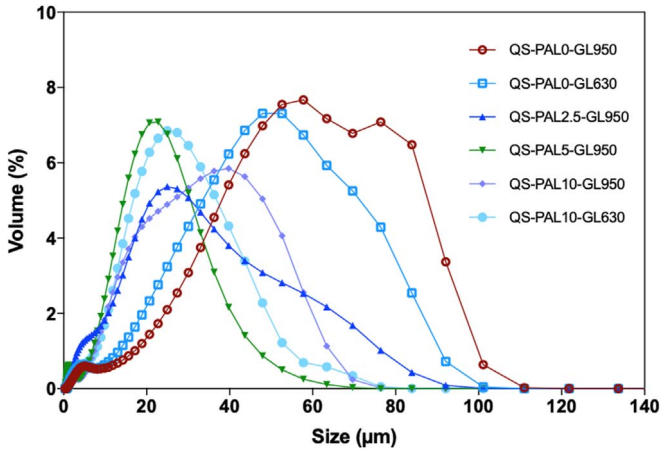

Figure 1. Particle size distribution for the QS and QS-PAL microspheres.

Table 1. Full factorial design matrix (CFD).

StdOrder	RunOrder	% PAL	ml GL
21	1	5	950
8	2	5	630
22	3	10	315
9	4	5	950
23	5	10	630
5	6	2.5	630
12	7	10	950
17	8	2.5	630
11	9	10	630
4	10	2.5	315
24	11	10	950
19	12	5	315
6	13	2.5	950
10	14	10	315
14	15	0	630
3	16	0	950
1	17	0	315
7	18	5	315
2	19	0	630
15	20	0	950
20	21	5	630
16	22	2.5	315
13	23	0	315
18	24	2.5	950

TIM release results were reported as the average release rate of 3 replicates. The release rate was calculated with the C_t/C_0 ratio, where C_t represents the concentration of TIM released at time t and C_0 represents the amount of TIM initially encapsulated. These results were adjusted using the following experimental models [26]:

2.9.1. First order release kinetics

$$F = F_W - Me^{-K_1 t}$$

where:

F: release rate (%); F_W: cumulative release amount (%); M: constant; K_1: first-order release rate constant; t: time.

Table 2. Composition of the selected microsphere formulations.

Formulations	PAL (%)	Glutaraldehyde (μl)
QS-PAL0-GL630	0	630
QS-PAL10-GL630	10	630
QS-PAL0-GL950	0	950
QS-PAL2.5-GL950	2.5	950
QS-PAL5-GL950	5	950
QS-PAL10-GL950	10	950

Table 3. Average particle size, swelling and absorption efficiency of the QS and QS-PAL microspheres.

Samples	Size (μm)	ED[a]
QS-PAL0-GL630	40.1	2.5
QS-PAL10-GL630	23.0	3.5
QS-PAL0-GL950	51.8	2.8
QS-PAL2.5-GL950	34.2	10.8
QS-PAL5-GL950	22.2	3.1
QS-PAL10-GL950	27.5	0.1

[a] Standard deviation.

2.9.2. Higuchi model

$$F = K_2 t^{1/2}$$

where:

F: release rate (%); K_2: release rate constant, t: time.

3. Results and discussion

3.1. Obtention of the QS and QS-PAL microspheres

The CFD was used to establish the effect of PAL, and GL (independent variables) on the emulsion process. Although this method is well known for chitosan microspheres [27–29], for the chitosan-palygorskite hybrid system, there are fewer [22, 25]. The CFD variables matrix used is presented in table 1; after the analysis of the experimental results, the formulations from table 2 were selected, mainly by considering the shape of the microspheres (perfect sphere) after incorporating palygorskite and the lowest microsphere agglomeration.

3.1.1. Particle size of the QS and QS-PAL microspheres

Table 3 presents the average particle size of the different formulations and the particle size distribution is presented in figure 1. The average particle sizes of the QS and QS-PAL microspheres (table 3) are in a range of 20 to 50 μm; the chitosan-only microspheres are those that presented a larger size. The size distribution of the hybrid microspheres shows less size polydispersity. For the formulations without the nanoclay (QS-PAL0-GL630 and QS-PAL0-GL950), a wide distribution is observed between 0.01 and 100 μm. However, when palygosrkite is incorporated, a narrower distribution is observed (for example 5% of PAL, from 0.01 to 83 μm). This indicates that palygorskite changes the emulsion behavior and its incorporation generates narrower and more uniform size distributions.

3.1.2. Morphology of the QS and QS-PAL microspheres

Figure 2 shows a sequence of SEM micrographs corresponding to the crosslinked formulations with 950 μl of GL with the different palygorskite contents: QS-PAL0-GL950 microspheres (figures 2(a) and (b)), QS-PAL2.5-GL950 (figures 2(c) and (d)), QS-PAL5-GL950 (figures 2(e) and (f)) and QS-PAL10-GL950 (figures 2(g) and (h)). Figure 3 shows the crosslinked formulations with 630 μl of GL. It is evident from the images, for both levels of crosslinking, the spherical morphology and the polydispersity of the microsphere sizes (table 2). The QS microspheres have a smooth and homogeneous surface. With 2.5, 5 and 10% of PAL they present irregularities on the surface which are accentuated as the nanoclay content increases. These results suggest that when the

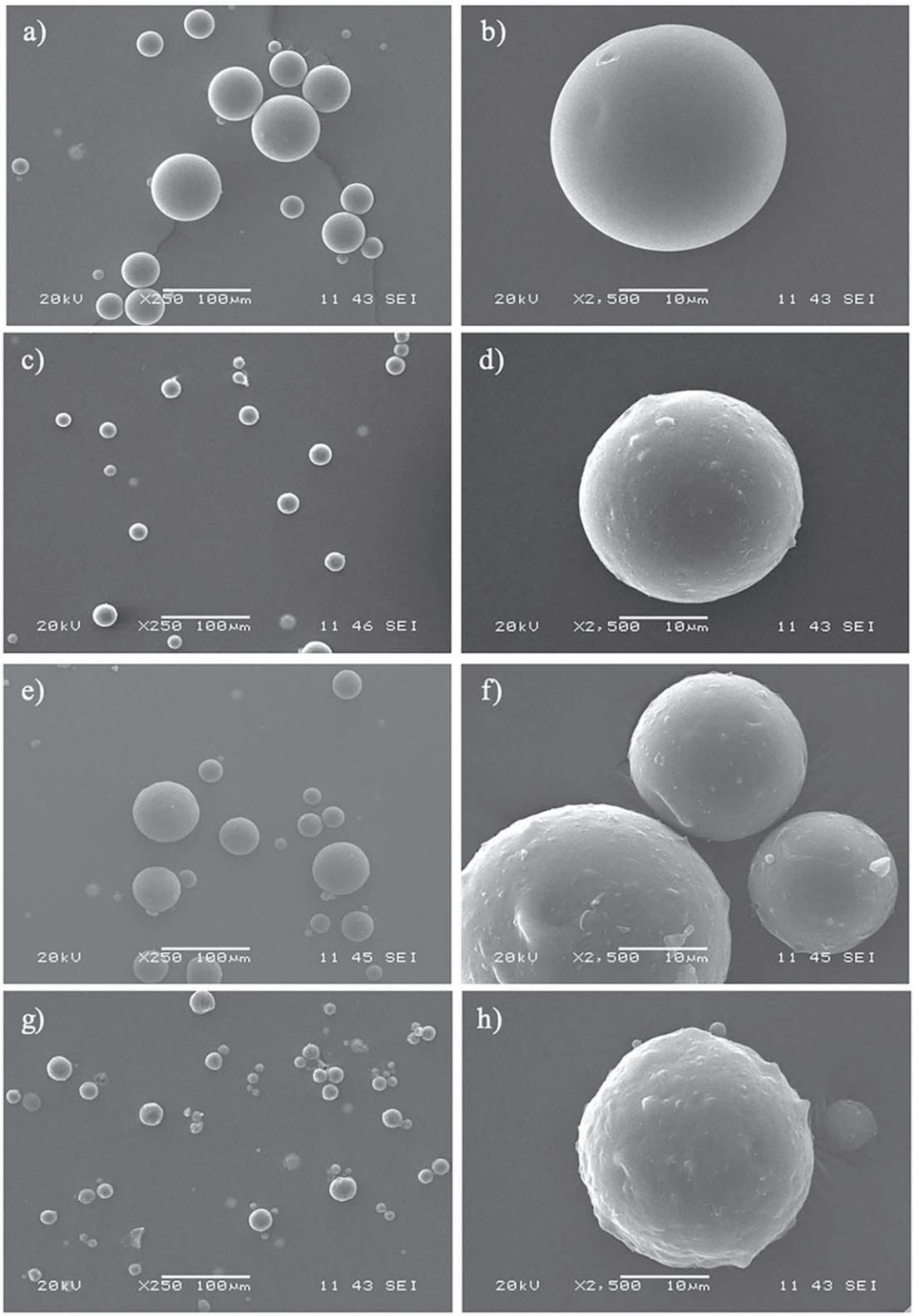

Figure 2. SEM micrographs. Crosslinked microspheres with GL 950 μl. (a) y (b) QS, (c) y (d) QS-PAL2.5, (e) y (f) QS-PAL5, (g) y (h) QS-PAL10.

emulsion is formed, PAL has a preference for the aqueous phases instead of the oil phase, due to the water affinity of its hydrophilic groups, as well as to its affinity with the functional groups -OH and -NH_2 of the chitosan [22–24].

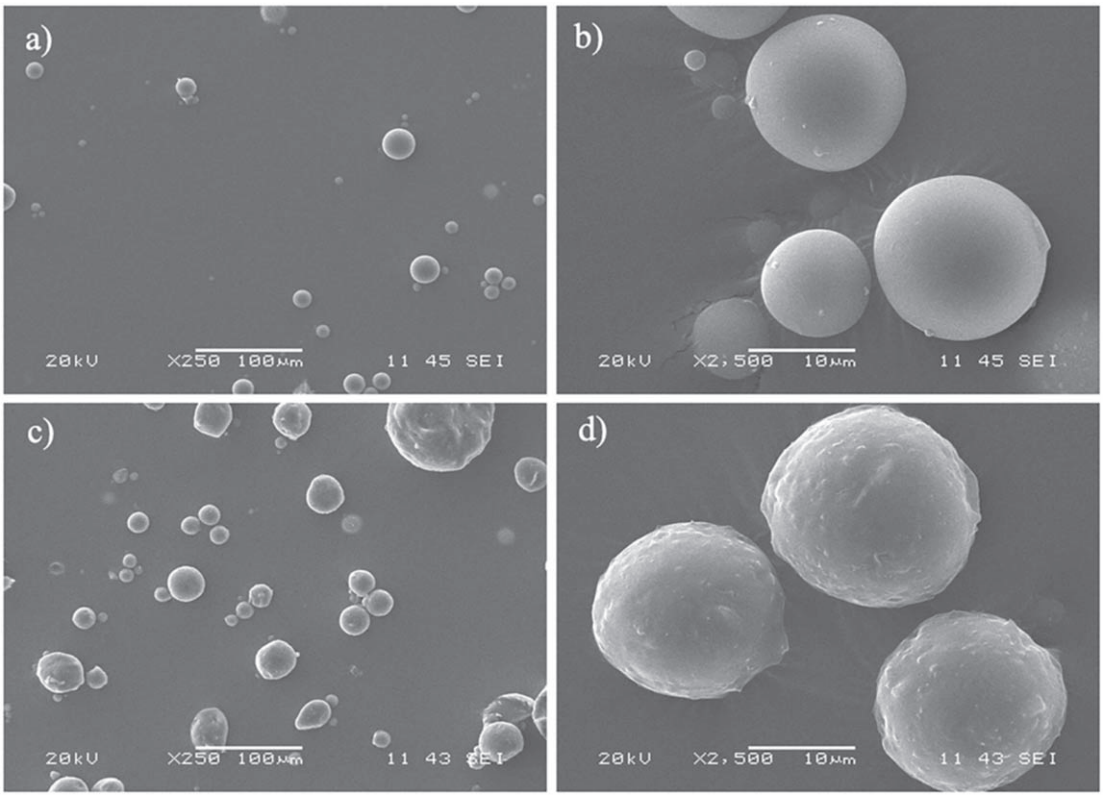

Figure 3. SEM micrographs of Crosslinked microspheres with GL 630 μl. (a) y (b) QS, (c) y (d) QS-PAL10.

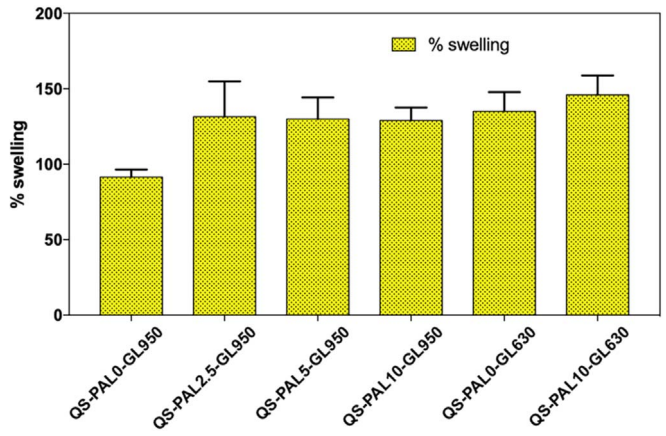

Figure 4. Percentage of swelling of QS and QS-PAL microspheres.

3.2. Characterization of the QS and QS-PAL microspheres

3.2.1. Swelling degree of the QS and QS-PAL microspheres

Figure 4 presents the swelling profiles of the microspheres QS and QS-PAL. The QS-PAL microspheres have a higher swelling rate than the QS microspheres. The amount of ethanol absorbed is related to the number of active groups in the microspheres. The addition of PAL increased the number of hydrophilic groups available in the structure of the microsphere.

The lowest degree of swelling, 88%, was from the microspheres without PAL cross-linked with 950 μl of GL, and the highest was 146% from the microspheres with 10% PAL crosslinked with 630 μl of GL. The glutaraldehyde reacts with the $-NH_2$ groups of the QS and as the amount of glutaraldehyde available in the emulsion increases, there are more crosslinked points in the polysaccharide chain, making the molecular network more rigid and decreasing the swelling ability of the microspheres. The crosslinked degree modifies the swelling percentage; also, in hybrid microspheres, the percentage of PAL influences the degree of swelling since it improves the interaction of the composite with ethanol by increasing the –OH groups available. The

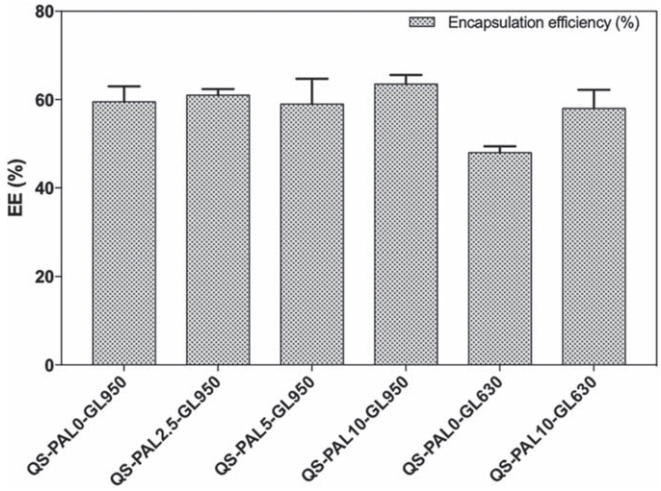

Figure 5. Encapsulation efficiency of QS and QS-PAL microspheres.

microsphere swelling is one of the parameters linked to the QS crosslinking and is directly related to the ability of the microsphere to trap TIM and, consequently, is also related to their release properties.

3.2.2. Encapsulation efficiency of thymol in QS and QS-PAL microspheres

Figure 5 shows the encapsulation efficiencies for the formulations analyzed. The results indicate that the microspheres with the highest degree of crosslinking (950 μl GL) and PAL content show some increase in their encapsulation efficiency compared to those crosslinked with 630 μl GL. The 630 μl GL formulations clearly show that the presence of PAL increases the encapsulation efficiency by around 16%. This could be due to the interaction between TIM and palygorskite since both contain –OH groups in their chemical structure. In addition, this phyllosilicate has a large surface area, micropores and channels (high porosity) [30], which influence the thymol retention (molecular size 10 Å) [31, 32]. The palygorskite has a high ability to absorb small molecules which could enter the internal gallery (around 11 Å) [24] and retain them inside the clay channels. Furthermore, –OH groups and unbalanced charges in crystal lattice defects (e.g. Si–O–Si) are additional sites for the absorption of different substances [33, 34].

3.2.3. FT-IR spectra of QS, PAL, TIM and microspheres QS and QS-PAL

Figures 6 and 7 present the FT-IR spectra of the QS, PAL, TIM and of the microspheres. The main bands of the QS spectrum in the 3750 to 3000 cm^{-1} range are due to stretching vibrations of the OH groups which overlap with the stretching vibration of N–H. The bands at 2875 and 2923 cm^{-1} correspond to the stretching of the C-H bond of the methylene and methyl groups, respectively [35]. The flexing vibrations of the methyl groups are also observed at 1424 cm^{-1} and methylenes at 1380 cm^{-1} [36]. The band observed at 1641 cm^{-1} can be assigned to the vibration –C=O of the secondary amide and that of 1318 cm^{-1} to $-CH_3$ of the tertiary amide. Also, the 1260 cm^{-1} band is assigned to the C–O–H vibration. The band at 1150 cm^{-1} is related to the asymmetric vibration of the C–O, those of 1065 and 1024 cm^{-1} can be related to the C–O vibrations of the COH, COC ring [37–40].

The purified PAL shows the main bands at 3616 cm^{-1} attributed to the stretching of Al–OH–Al, at 3690 and 3584 cm^{-1} assigned to the stretching vibrations of Mg^3–OH, Al–$OHFe^{3+}$, respectively. Absorption bands between 3700 and 3200 cm^{-1} are generally assigned to the stretching vibrations of structural –OH and hygroscopic water [41, 42]. The band between 1600–1700 cm^{-1} corresponds to the bending-type vibrations of the –OH of the coordinated, absorbed and zeolitic water; the band at 1445 cm^{-1} is attributed to the bending vibration of the –OH of the structural water and zeolitic [43, 44]. The region at 1300–1000 cm^{-1} is assigned to the movements and vibrations of the Si–O bond.

The TIM has a wide band in the range of 3500 to 3200 cm^{-1}, a characteristic of the O-H group. The stretching of aromatic or unsaturated C–H is observed at 3075 cm^{-1}; at 2962 and 2872 cm^{-1} the characteristic bands of the methyl $-CH_3$ asymmetric and symmetrical stretching appear, respectively. The peaks at 1590 and 1517 cm^{-1} correspond to the symmetric and asymmetric stretches of the aromatic ring, and the asymmetric flexion of methyl $-CH_3$ is at 1455 cm^{-1} [45–47].

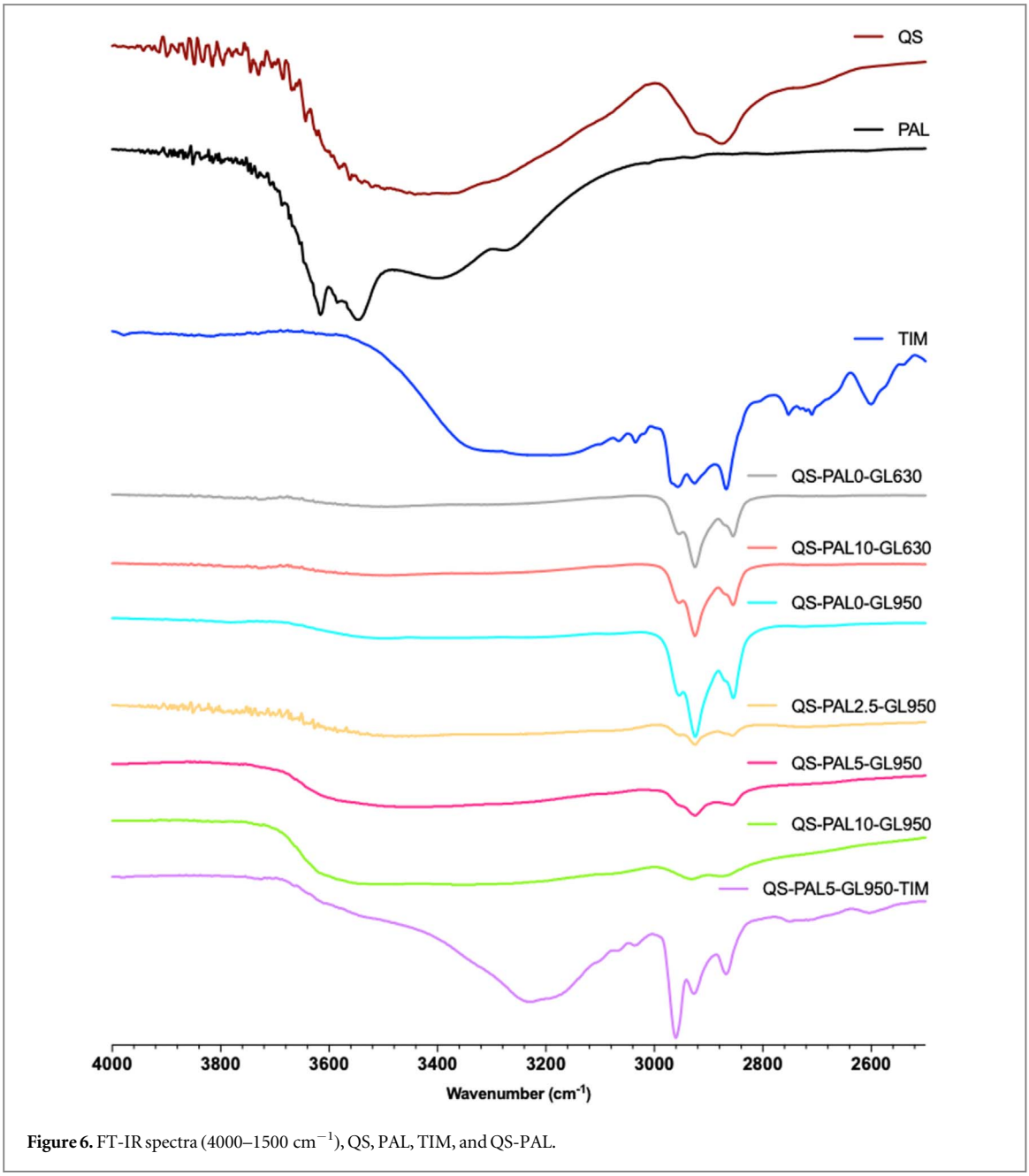

Figure 6. FT-IR spectra (4000–1500 cm^{-1}), QS, PAL, TIM, and QS-PAL.

Each of the components in the hybrid microspheres have characteristic bands in the IR spectra, the overlap of these bands does not make the presence of PAL so evident in hybrid materials. However, subtle changes of certain band intensities are observed between 3000 and 3750 cm^{-1} at the microspheres spectra of QS-PAL10-GL630, QS-PAL2.5-GL950, QS-PAL5-GL950, QS-PAL10-GL950, which may be due to the presence of the nanoclay. On the other hand, the characteristic bands of the TIM at 736 and 808 cm^{-1} corresponding to ring flexion, the asymmetric flexion of methyl, $-CH_3$ at 1455 cm^{-1} and the increase in the intensity of the band at 3200–3500 cm^{-1} (OH) are evidence of the presence of this compound in the microspheres.

3.2.4. X-ray diffraction (XRD) of QS, PAL and of the microspheres of QS, QS-PAL

Figure 8 presents the X-ray diffraction patterns of the QS, PAL, and the microspheres from table 2: QS-PAL0-GL630, QS-PAL10-GL630, QS-PAL0-GL950, QS-PAL2.5-GL950, QS-PAL5-GL950, QS-PAL5-GL-950-TIM and QS-PAL10-GL950. Two crystalline reflections for the QS are observed in the 2θ interval from 7 to 25°. These signals are attributed to the packed macromolecular chains resulting from the intermolecular hydrogen bridges with the NH_2 groups generated during the deacetylation process [48]. However, the GL crosslinked microspheres have none of these signals and only show the amorphous phase signal.

The XRD pattern of the PAL shows the strongest peaks at (2θ) 8.4, 13.9, 16.4, 19.8, 20.8, 24.2, 26.6, 28.8, and 35.3°. They correspond to the crystallographic planes (110), (200), (130), (040), (121), (240), (400), (231) and

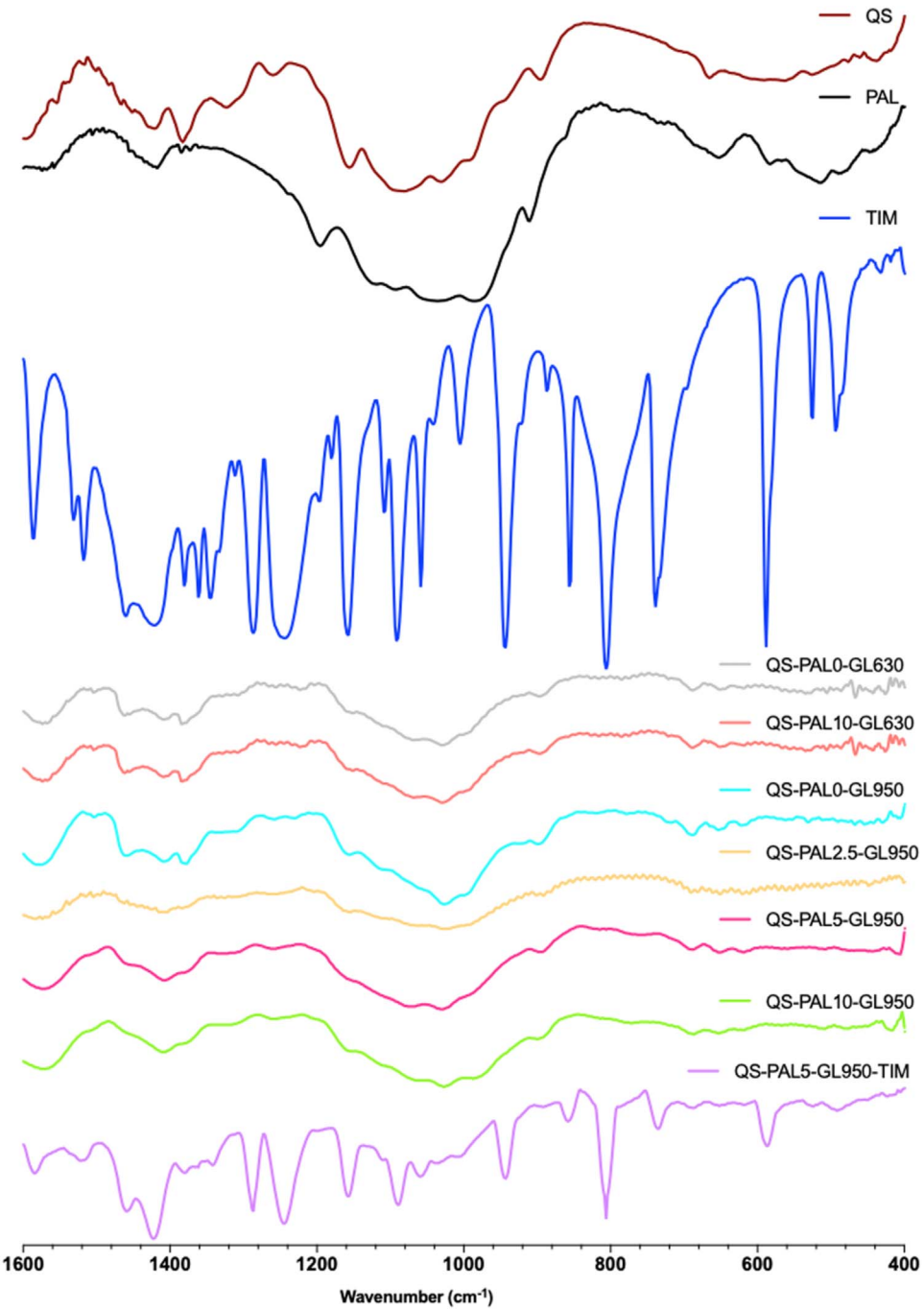

Figure 7. FT-IR spectra (1600–400 cm^{-1}), QS, PAL, TIM, and QS-PAL.

(061) with their respective interplanar distances at $d_{110} = 1{,}054$, $d_{200} = 0.643$, $d_{130} = 0.538$, $d_{040} = 0.446$, $d_{121} = 0.429$, $d_{240} = 0.367$, $d_{400} = 0.324$, $d_{231} = 0.324$ and $d_{061} = 0.253$ nm [49, 50].

The XRD patterns of the crosslinked microspheres QS-PAL0-GL950 and QS-PAL0-GL630 without PAL do not show the characteristic peaks of the QS. During the emulsion and in the crosslinking reaction the crystalline structures were disordered, resulting in an amorphous material.

The hybrid and crosslinked microspheres with 950 μL of GL, QS-PAL2.5-GL-950, QS-PAL5-GL950 and QS-PAL10-GL950 have a strong band at 2θ 8.4° (110) and weaker signals in the range 15°–36° corresponding to the PAL. These signals of the crosslinked microspheres prove the PAL presence in these nanostructured materials. Furthermore, the increase of the band intensity at 2θ 8.4° (110) is related to the PAL content increment in the microspheres, where a stronger signal for the formulation with 10% PAL is observed. Similarly, for QS-PAL10-GL630, the PAL signal at 2θ 8.4° (110) proves that at this crosslinking level, it is possible to incorporate PAL into the microspheres.

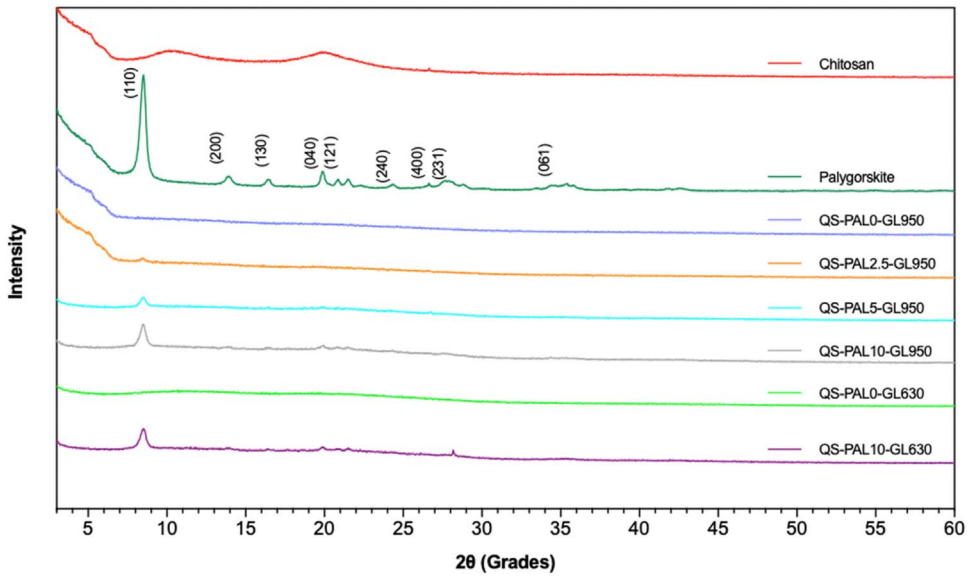

Figure 8. XRD diffractograms of QS, PAL, QS-PAL0-GL950, QS-PAL2.5-GL950, QS-PAL5-GL-950, QS-PAL10-GL950, QS-PAL0-GL630 y QS-PAL10-GL630.

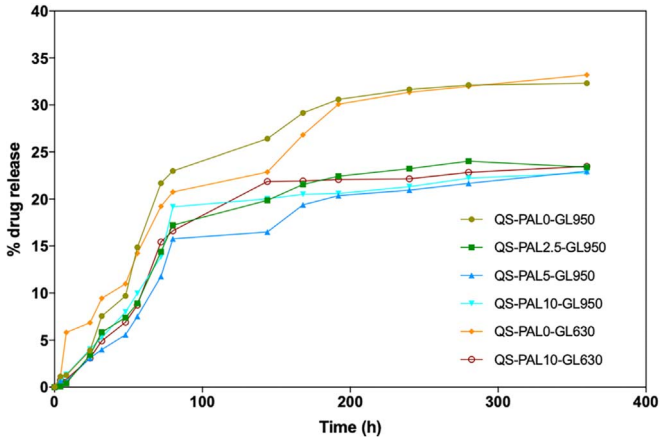

Figure 9. Thymol release isotherms in QS, QS-PAL microspheres.

3.3. TIM delivery isotherms of QS and QS-PAL microspheres

Figure 9 presents the results of the environmental release of absorbed TIM in the microspheres QS-PAL0-GL950, QS-PAL2.5-GL950, QS-PAL5-GL-950, QS-PAL10-GL950, QS-PAL0-GL630 and QS-PAL10-GL630.

The formulations without PAL (QS-PAL0-GL630 and QS-PAL0-GL950) showed similar behavior; during the first 70 h a fast release greater than 15 and 20% was observed, however, during the first 8 h, the release rate is faster for QS-PAL0-GL630, which could be attributed to the greater swelling presented by this formulation (table 3). After 72 h of release, the release rate gradually lowers for these two formulations until reaching 30% of released TIM.

The hybrid microspheres presented during the initial times (48 h) a fast release rate up to about 12% TIM. Then the release rate gradually reached a maximum at approximately 20% TIM which is lower than the maximum presented by the microspheres without PAL (QS-PAL0-GL950 and QS-PAL0-GL630 - around 30%). These results proved that the PAL in the microspheres changed the TIM delivery rate; it is evident that the TIM release profiles are modified, showing a slower delivery rate to the environment due to the molecular interaction between the TIM –OH groups with the –OH and $–NH_2$ of the QS, and to the nanoclay physical interactions between the –OH of PAL and the TIM, which restrict its mobility and result in a slower delivery rate.

The initial fast release rate can be attributed to the release of TIM adsorbed on the microspheres surface. The TIM delivery rate is affected by the PAL content, as well as by the cross-linking that generates a compact network of biopolymer chains; these factors create a physical and chemical interaction with TIM, resulting in a slower mobility and diffusion in the microspheres. In general, the results demonstrate that the incorporation of PAL

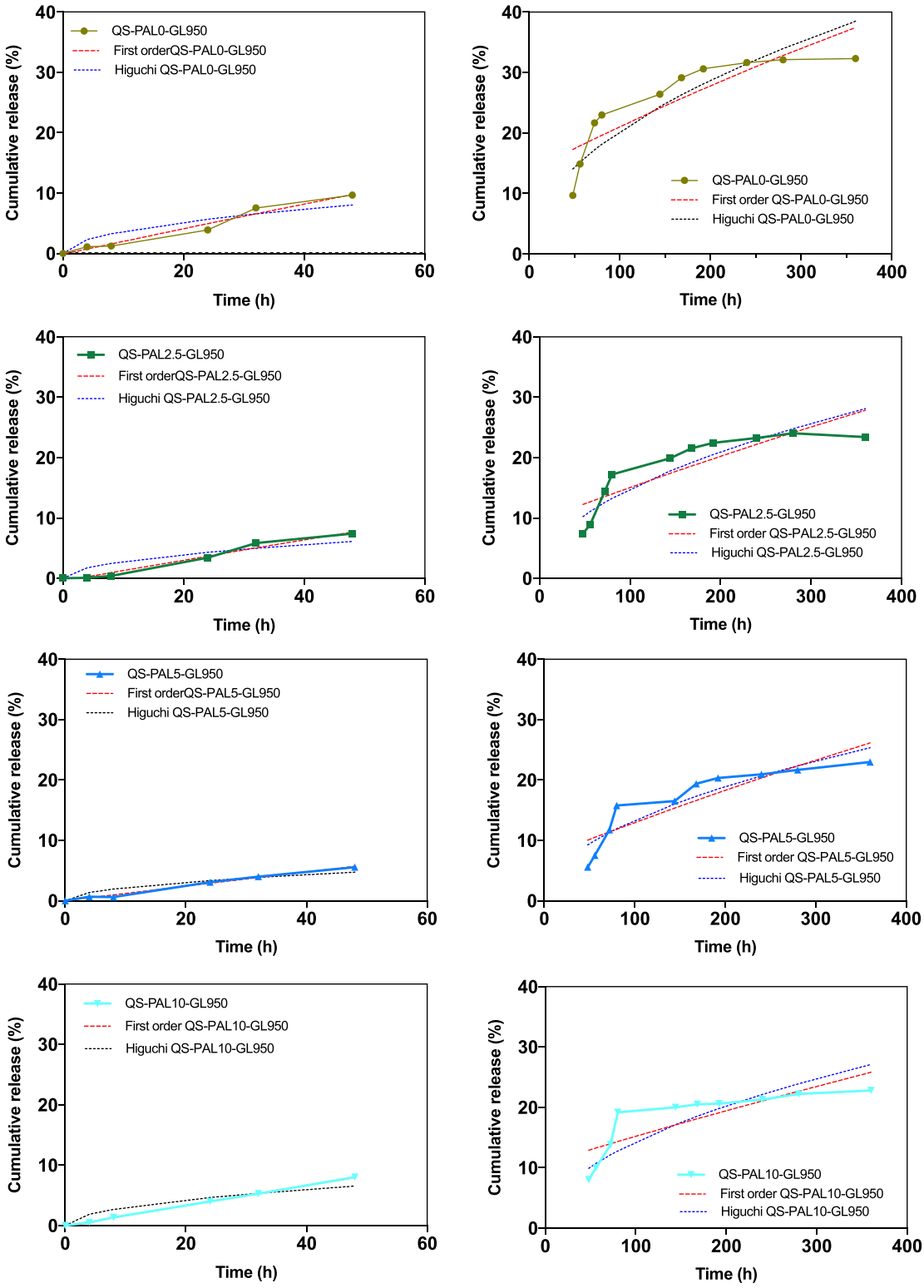

Figure 10. Thymol release isotherms in QS and QS-PAL microspheres, QS-PAL0-GL950, QS-PAL2.5-GL950, QS-PAL5-GL950 QS-PAL10-GL950.

can improve the controlled delivery properties of the QS microspheres. Furthermore, one of the current problems with the use of TIM to control the *Varroa destructor* mite is the concentration used; a high level of TIM causes lack of control in the hive, increased aggressiveness of the bees and displacement of the young bees (pupaes), making the controlled delivery of this active agent an attractive method to reduce its side effects in the apiaries [2, 51].

The controlled release of an active agent is the result of the diffusion phenomenon of this in the carrier, which can be a polymer, an inorganic compound or a hybrid material, as well as is result of the mass transfer

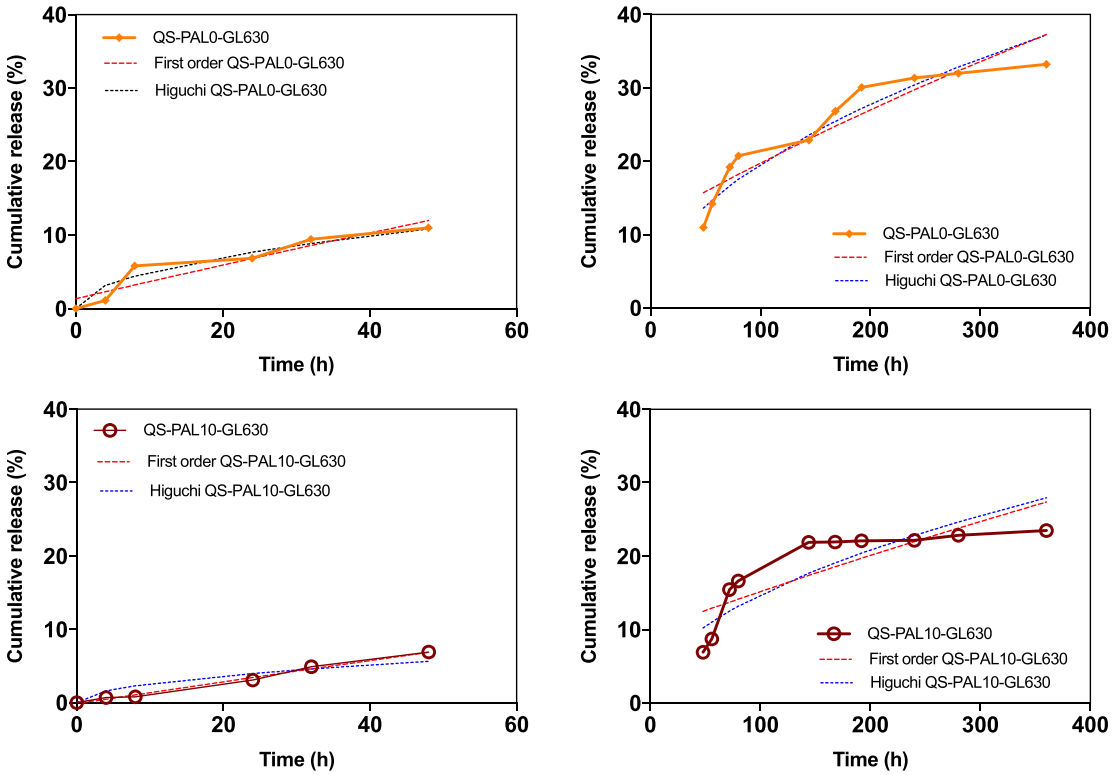

Figure 11. Thymol release isotherms in QS and QS-PAL microspheres, QS-PAL0-GL630, QS-PAL10-GL630.

Table 4. Initial fit models for TIM release kinetic data.

System	Model	Equation	S
QS-PAL0-GL950	First order	F = 100–95.2404e^(−0.00137974t)	5.40
	Higuchi	F = 1.9879t^(1/2)	3.78
QS-PAL2.5-GL950	First order	F = 100–96.49944e^(−0.000936698t)	4.10
	Higuchi	F = 1.45197t^(1/2)	2.81
QS-PAL5-GL950	First order	F = 100–97.2959e^(−0.000859275t)	3.30
	Higuchi	F = 1.30618t^(1/2)	2.47
QS-PAL10-GL950	First order	F = 100–95.7821e^(−0.00084549t)	4.24
	Higuchi	F = 1.40489t^(1/2)	2.47
QS-PAL0-GL630	First order	F = 100–94.3999e^(−0.00128337t)	4.02
	Higuchi	F = 1.94771t^(1/2)	2.24
QS-PAL10-GL630	First order	F = 100–96.3631e^(−0.000918529t)	4.33
	Higuchi	F = 1.44206t^(1/2)	3.06

restrictions at the interface carrier/medium. The design and modification of a controlled release system requires knowledge of the diffusion mechanism of the active agent through the carrier. Therefore, to understand the release behavior of TIM in QS microspheres, the experimental data of its release shown in figure 9 were adjusted to different mathematical models to analyze the kinetics and release mechanisms: first-order and Higuchi models are frequently used models. The model fit and the standard error of non-linear regression (S) are shown in table 4. A small S indicates that the experimental values fit better to the theoretical lines; in addition, the use of S is more convenient than r^2 to determine the precision predictions of the mathematical models [52]. The S values shown in table 4 are relatively high for both models, so they do not fit well enough, the Higuchi model, however, has the best fit. Figure 9 shows that the TIM release curves could be divided into two sections, as shown in figures 10 and 11: a first burst release stage and a second slow release stage [26]. By making this division it is intended to achieve a better fit applying the models by sections. The new values of S are presented in table 5.

The two-stage TIM release process may be due to a high concentration gradient between the environment and the microspheres, along with the release of absorbed TIM on microsphere surfaces. The next release stage (slow) has a lower concentration gradient and a greater resistance of the TIM to get out into the medium since

Table 5. Step-fit models for thymol release kinetic data.

System	Model	Equation	S
First stage			
QS-PAL0-GL950	First order	F = 100–101.127e^(−0.00217195t)	0.76
	Higuchi	F = 1.16324t^(1/2)	1.57
QS-PAL2.5-GL950	First order	F = 100–100.4656e^(−0.00176298t)	0.57
	Higuchi	F = 0.882417t^(1/2)	1.44
QS-PAL5-GL950	First order	F = 100–99.9877e^(−0.00122406t)	0.24
	Higuchi	F = 0.685456t^(1/2)	0.76
QS-PAL10-GL950	First order	F = 100–100.0796e^(−0.0017443t)	0.08
	Higuchi	F = 0.947687t^(1/2)	1.11
QS-PAL0-GL630	First order	F = 100–98.6497e^(−0.00237542t)	1.71
	Higuchi	F = 1.56714t^(1/2)	1.19
QS-PAL10-GL630	First order	F = 100–100.11e^(−0.00151215t)	0.29
	Higuchi	F = 0.815615t^(1/2)	1.05
Second stage			
QS-PAL0-GL950	First order	F = 100–86.3435e^(−0.000895663t)	4.20
	Higuchi	F = 2.02909t^(1/2)	3.69
QS-PAL2.5-GL950	First order	F = 100–90.4343e^(−0.000627378t)	3.38
	Higuchi	F = 1.48103t^(1/2)	2.75
QS-PAL5-GL950	First order	F = 100–92.725e^(−0.000632636t)	2.97
	Higuchi	F = 1.33538t^(1/2)	2.32
QS-PAL10-GL950	First order	F = 100–89.2477e^(−0.000512976t)	3.24
	Higuchi	F = 1.42995t^(1/2)	3.03
QS-PAL0-GL630	First order	F = 100-88.2003e^(−0.000947196t)	3.01
	Higuchi	F = 1.96402t^(1/2)	2.41
QS-PAL10-GL630	First order	F = 100–90.0654e^(−0.000598385t)	3.72
	Higuchi	F = 1.47336t^(1/2)	3.14

the distance that the TIM molecules have to travel is greater than in the burst release stage. Also, in the diffusion route, the PAL makes the diffusion more difficult. Figures 10 and 11 graphically show the isotherm profile analysis by release stage of the experimental data as well as the fit lines corresponding to the mathematical models for the microspheres QS-PAL0-GL950, QS-PAL2.5-GL950, QS-PAL5-GL950 QS-PAL10-GL950 and QS-PAL0-GL630, QS-PAL10-GL630. It can be seen in both figures and considering S, that, separating the experimental data by stages, the first order model presents a good fit in the first release stage and the Higuchi model shows better fit to the second release stage, compared to the total analysis of the data.

4. Conclusions

Chitosan microspheres, and chitosan hybrid microspheres with 2.5, 5 and 10% palygorskite were successfully prepared by the emulsion method and used as matrices for the controlled delivery of thymol. The morphology of the hybrid microspheres depends significantly on the amount of palygorskite incorporated into the system: a smooth and homogeneous surface was observed for the cross-linked spheres without nano-clays, and a rough and heterogeneous surface in the hybrid microspheres. Average particle sizes ranged from 20 to 50 μm. The incorporation of PAL to the microspheres reduces their average size and their size polydispersity. The FTIR analyses showed the presence of the nanoclay in the microspheres, and XRD confirmed this fact.

The results obtained demonstrated that the hybrid microspheres exhibit slower and more sustained thymol release profiles than the pristine chitosan microspheres, which is attributable to the interactions of thymol with the functional groups of both the palygorskite and the matrix. Based on the experimental results, it can be concluded that hybrid microspheres loaded with thymol could be potential candidates for the thymol controlled release as a potential system for pest control applications in hives.

A two-stages release process were observed in the TIM release isotherms. The S values suggest that the analysis by two stages is more appropriate for the release behavior of thymol. The S statistic showed that the first order model presented a better adjustment for the first stage, related to the fast release of the thymol absorbed in the microspheres surface. But none of the models used fitted well the second release stage.

Acknowledgments

The authors appreciate the technical assistance of Santiago Duarte Aranda for the SEM analysis, Mirbella Cáceres Farfán for infrared spectroscopy technical support, Dr Gonzalo Canché Escamilla for important comments.

Data availability statement

All data that support the findings of this study are included within the article (and any supplementary files).

Credit author statement

P I Gonzalez-Chi: Conceptualization, Supervision, Writing - Review & Editing. **Rocío Borges-Argáez:** Conceptualization, Supervision, Writing - Review & Editing. **W Ramos-Torres:** Visualization, Methodology, Investigation, Writing - Original Draft.

Funding

This research did not receive any specific grant from funding agencies in the public, commercial, or not-for-profit sectors.

Declaration of conflicting interests

The author(s) declared no potential conflicts of interest with respect to the research, authorship, and/or publication of this article.

ORCID iDs

P I Gonzalez-Chi https://orcid.org/0000-0002-5917-078X

References

[1] Orzali L, Corsi B, Forni C and Riccioni L 2017 Chitosan in agriculture: a new challenge for managing plant disease *Biological Activities and Application of Marine Polysaccharides*ed E Shalaby (United States of America: IntechOpen) 17–36
[2] Dwijendra S 2006 *Advances in Plant Breeding* 1st edn (Uttar Pradesh, India: Springer) (https://doi.org/10.1007/978-3-319-22521-0)
[3] Rosenkranz P, Aumeier P and Ziegelmann B 2010 Biology and control of Varroa destructor *J. Invertebr. Pathol.* **103** S96–119
[4] Rice N D, Winston M L, Whittington R and A Higo H 2002 Comparison of release mechanisms for botanical oils to control Varroa destructor (Acari: Varroidae) and Acarapis woodi (acari: Tarsonemidae) in colonies of honey bees (Hymenoptera: Apidae) *J. Econ. Entomol.* **95** 221–6
[5] Ruffinengo S R, Maggi M D, Fuselli S, De Piano F G, Negri P, Brasesco C, Satta A, Flores I and Eguaras M J 2014 *Bioactivity of Microencapsulated Essentials Oils and Perspectives of their use in the Control of Varroa Destructor* **67** 81–6
[6] Ferrer-Dufol M, Martinez-Vin¯uales A I and Sanchez-Acedo C 1991 Comparative tests of fluvalinate and flumethrin to control Varroa jacobsoni Oudemans *J. Apic. Res.* **30** 103–6
[7] Abdelmir M, Medina, De W, Jorge J M-I and Olivares J C M 2007 Effectiveness of a thymol based gel for the control of Varroa destructor mite that infests Apis mellifera honey bee colonies, under tropical conditions in Yucatan, Mexico *Vet. Mexico* **38** 1–9
[8] Isman M B 2006 Botanical insecticides, deterrents, and repellents in modern agriculture and an increasingly regulated world *Annu. Rev. Entomol.* **51** 45–66
[9] Lambert R J, Skandamis P N, Coote P J and Nychas G J E 2001 A study of the minimum inhibitory concentration and mode of action of oregano essential oil, thymol and carvacrol *J. Appl. Microbiol.* **91** 453–62
[10] Martins I M, Barreiro M F, Coelho M and Rodrigues A E 2014 Microencapsulation of essential oils with biodegradable polymeric carriers for cosmetic applications *Chem. Eng. J.* **245** 191–200
[11] Lewis D H and Cowsar D R 1977 Principles of controlled release pesticides *Int. Control. Release Pestic. Symp.* 1–16
[12] Yang F L, Li X G, Zhu F and Lei C L 2009 Structural characterization of nanoparticles loaded with garlic essential oil and their insecticidal activity against Tribolium castaneum (Herbst) (Coleoptera: Tenebrionidae) *J. Agric. Food Chem.* **57** 10156–62
[13] Ganguly K, Aminabhavi T M and Kulkarni A R 2011 Colon targeting of 5-fluorouracil using polyethylene glycol cross-linked chitosan microspheres enteric coated with cellulose acetate phthalate *Ind. Eng. Chem. Res.* **50** 11797–807
[14] Paula H C B, Sombra F M, Cavalcante R D F, Abreu F O M S and Paula R C D 2011 Preparation and characterization of chitosan/cashew gum beads loaded with Lippia sidoides essential oil *Mater. Sci. Eng.* C **31** 173–8
[15] Velásquez C L 2003 Algunos usos del quitosano en sistemas acuosos *Rev. Iberoam. Polímeros.* **4** 91–109
[16] Ha J U and Xanthos M 2011 Drug release characteristics from nanoclay hybrids and their dispersions in organic polymers *Int. J. Pharm.* **414** 321–31

[17] Jain S and Datta M 2015 Oral extended release of dexamethasone: montmorillonite-PLGA nanocomposites as a delivery vehicle *Appl. Clay Sci.* **104** 182–8
[18] Wang Q, Wu J, Wang W and Wang A 2011 Preparation, characterization and drug-release behaviors of crosslinked chitosan/attapulgite hybrid microspheres by a facile spray-drying technique *J. Biomater. Nanobiotechnol.* **02** 250–7
[19] Liu K-H, Liu T-Y, Chen S-Y and Liu D-M 2008 Drug release behavior of chitosan–montmorillonite nanocomposite hydrogels following electrostimulation *Acta Biomater.* **4** 1038–45
[20] Jafarbeglou M, Abdouss M, Shoushtari A M and Jafarbeglou M 2016 Clay nanocomposites as engineered drug delivery systems *R. Soc. Chem.* **6** 50002–16
[21] Viseras C, Aguzzi C, Cerezo P and Bedmar M C 2008 Biopolymer clay nanocomposites for controlled drug delivery *Mater. Sci. Technol.* **24** 1020–6
[22] Alcântara A C S, Darder M, Aranda P and Ruiz-Hitzky E 2014 Polysaccharide-fibrous clay bionanocomposites *Appl. Clay Sci.* **96** 2–8
[23] Ruiz-Hitzky E, Darder M, Fernandes F M, Wicklein B, Alcântara A C S and Aranda P 2013 Fibrous clays based bionanocomposites *Prog. Polym. Sci.* **38** 1392–414
[24] Singer A and Galán Huertos E 2011 *Developments in Palygorskite-Sepiolite Research: a New Outlook on these Nanomaterials* (Amsterdam: Elsevier)
[25] Wu J, Ding S, Chen J, Zhou S and Ding H 2014 Preparation and drug release properties of chitosan/organomodified palygorskite microspheres *Int. J. Biol. Macromol.* **68** 107–12
[26] Liao K, Li P, Chen G and Qiu X 2019 Preparation and release properties of flufiprole-loaded microcapsules with core status of solid particles, solution droplets and oil suspending agent *J. Macromol. Sci. Part A Pure Appl. Chem.* **56** 171–8
[27] Sanna V, Roggio A M, Pala N, Marceddu S, Lubinu G, Mariani A and Sechi M 2015 Effect of chitosan concentration on PLGA microcapsules for controlled release and stability of resveratrol *Int. J. Biol. Macromol.* **72** 531–6
[28] Agnihotri S A, Mallikarjuna N N and Aminabhavi T M 2004 Recent advances on chitosan-based micro- and nanoparticles in drug delivery *J. Control. Release* **100** 5–28
[29] Hafizah F, Yusop M, Fairuz S, Manaf A and Hamzah F 2017 Preservation of Bioactive Compound via Microencapsulation *Chem. Eng. Res. Bull.* **19** 50–6
[30] Galan E 1996 Properties and applications of palygorskite-sepiolite clays *Clay Miner.* **31** 443–53
[31] Corma E S A and Mifsud A 1987 Influence of the chemical composition ans textural characterisrtics of palygorskite on the acid leaching of octahedral cations *Clay Miner.* **22** 225–32
[32] Corma A and Mifsud A 1990 Kinetics of the acid leaching of palygorskite: influence of the octahedral sheet composition *Clay Miner.* **25** 197–205
[33] Abdul-Latif N and Weaver C E 1969 Kinetics of acid-dissolution of palygorskite (attapulgite) and sepiolite *Clays Clay Miner.* **17** 169–78
[34] Gonzalez F, Pesquera C, Blanco C, Benito I, Mendioroz S and Pajares J A 1990 Structural and textural evolution under thermal treatment of natural and acid-activated Al-rich and Mg-rich palygorskites *Appl. Clay Sci.* **5** 23–36
[35] Silva S M L, Braga C R C, Fook M V L, Raposo C M O, Carvalho L H and Canedo E L 2012 *Infrared Spectroscopy-Materials Science, Engineering and Technology Edited* 1st edn (Brazil: IntechOpen) (https://doi.org/10.5772/46845)
[36] Mano J F, Koniarova D and Reis R L 2003 Thermal properties of thermoplastic starch/synthetic polymer blends with potential biomedical applicability *J. Mater. Sci. Mater. Med.* **14** 127–35
[37] Paluszkiewicz C, Stodolak E, Hasik M and Blazewicz M 2011 FT-IR study of montmorillonite-chitosan nanocomposite materials *Spectrochim. Acta - Part A Mol. Biomol. Spectrosc.* **79** 784–8
[38] Marchessault R H, Bremner G and Chauve G 2006 *Polysaccharides for Drug Delivery and Pharmaceutical Applications* 934 (United States of America: ACS Symposium Series) 6 121–37
[39] Xu Y X, Kim K M, Hanna M A and Nag D 2005 Chitosan-starch composite film: preparation and characterization *Ind. Crops Prod.* **21** 185–92
[40] Yuan Q, Shah J, Hein S and Misra R D K 2010 Controlled and extended drug release behavior of chitosan-based nanoparticle carrier *Acta Biomater.* **6** 1140–8
[41] Antonio S-M G, Iván G-C P and Luis G-R J 2015 Influence of chemically treated palygorskite over the rheological behavior of polypropylene nanocomposites *Ing. Investig. y Tecnol.* **16** 491–501
[42] Yan W, Liu D, Tan D, Yuan P and Chen M 2012 FTIR spectroscopy study of the structure changes of palygorskite under heating *Spectrochim. Acta - Part A Mol. Biomol. Spectrosc.* **97** 1052–7
[43] Suárez M and García-Romero E 2006 FTIR spectroscopic study of palygorskite: influence of the composition of the octahedral sheet *Appl. Clay Sci.* **31** 154–63
[44] Cisneros D E 2017 Estudio de la dispersión de paligorskita en matrices poliméricas de Poliamida 6 y Polipropileno mediante mezclado en fundido, PhD Thesis, Centro de Investigación Científica de Yucatán
[45] Bounaas K, Bouzidi N, Daghbouche Y, Garrigues S, De La Guardia M and El Hattab M 2017 Fourier transform infrared analysis of commercial formulations for: Varroa treatment *Anal. Methods* **9** 1–9
[46] Zamani Z, Alipour D and Reza H 2015 *Development and Evaluation of Thymol Microparticles Using Cellulose Derivatives as Controlled Release Dosage Form* **14** 1031–40
[47] Schulz H, Schrader B, Quilitzsch R, Pfeffer S and Krüger H 2003 Rapid classification of basil chemotypes by various vibrational spectroscopy methods *J. Agric. Food Chem.* **51** 2475–81
[48] Santana A C S G V, Sobrinho J L S, da Silva Filho E C and Nunes L C C 2017 Obtaining the palygorskite:chitosan composite for modified release of 5-aminosalicylic acid *Mater. Sci. Eng.* C **73** 245–51
[49] Xi Y, Mallavarapu M and Naidu R 2010 Adsorption of the herbicide 2,4-D on organo-palygorskite *Appl. Clay Sci.* **49** 255–61
[50] Yan W, Yuan P, Chen M, Wang L and Liu D 2013 Infrared spectroscopic evidence of a direct addition reaction between palygorskite and pyromellitic dianhydride *Appl. Surf. Sci.* **265** 585–90
[51] Espinosa-Montaño L G and Guzmán-Novoa E 2007 Effectiveness of two natural miticides, formic acid and thymol, for control of the mite Varroa destructor in honey bees (Apis mellifera L.) in Villa Guerrero, Mexico *Vet. Mexico* **38** 9–19
[52] Spiess A N and Neumeyer N 2010 An evaluation of R2as an inadequate measure for nonlinear models in pharmacological and biochemical research: a Monte Carlo approach *BMC Pharmacol.* **10** 1–11